AAS 19-808

DYNAMICAL STRUCTURES NEARBY NRHOS WITH APPLICATIONS IN CISLUNAR SPACE

Emily M. Zimovan-Spreen* **and Kathleen C. Howell†**

The development of a methodology to move through cislunar space along fundamental dynamical paths is relevant to NASA's cislunar transportation network goals. To enable an informed design approach for transfer trajectories departing from or arriving at a Near Rectilinear Halo Orbit (NRHO), higher-period orbits that bifurcate from the NRHO region of the halo orbit family are combined with other known structures, such as Lagrange point and resonant orbits, in the Earth-Moon neighborhood. As a consequence of this design strategy, novel impulsive transfer options between NRHOs and distant retrograde orbits that possess predictable geometries are constructed.

INTRODUCTION

An enduring human presence in the regions beyond Low Earth Orbit (LEO) is viewed by NASA and a variety of private organizations as an essential step in the development of a robust space economy and the evolution of manned missions to Mars. A dynamical understanding of orbits in the Earth-Moon neighborhood that can sustain long-term activities and trajectories that link locations of interest forms a critical foundation for the creation of an orbital infrastructure to support a lasting human presence. The Gateway, a future long-term habitat or hub in an orbit near the Moon, is expected to serve as a staging location for activities and missions within cislunar space; the current orbit of interest for this endeavor is a Near Rectilinear Halo Orbit (NRHO).[1]

Expanding beyond this hub near the Moon, NASA's goals for the Deep Space Transport (DST) include a transportation network linking locations in cislunar and translunar space within the next decade using both electric and chemical propulsion.[2,3] Due to an interest in long-term activities, stable or nearly-stable periodic orbits, (e.g., Distant Retrograde Orbits (DROs) and NRHOs, appearing in Figure 1) offer potential utility, however, transfer design between these types of orbits presents challenges. In particular, stable and unstable invariant manifolds, typically leveraged for initial guess generation in transfer design, are either non-existent or not well-defined. In response, multiple authors have produced various alternative strategies for both impulsive and low-thrust transfers between stable and nearly-stable orbits. Examples include work by Capdevila et al. to generate a network of impulsive transfers between stable periodic orbits in cislunar space,[4] Parker et al. and Herman investigating low-thrust transfers from Earth to DROs,[5,6] and work by Parrish et al. developing low-thrust transfers between DROs and L_2 halo orbits (beyond the region of NRHOs).[7]

*Ph.D. Student, School of Aeronautics and Astronautics, Purdue University, 701 W. Stadium Avenue, West Lafayette, IN 47907-2045

†Hsu Lo Distinguished Professor of Aeronautics and Astronautics, Purdue University, 701 W. Stadium Avenue, West Lafayette, IN 47907-2045

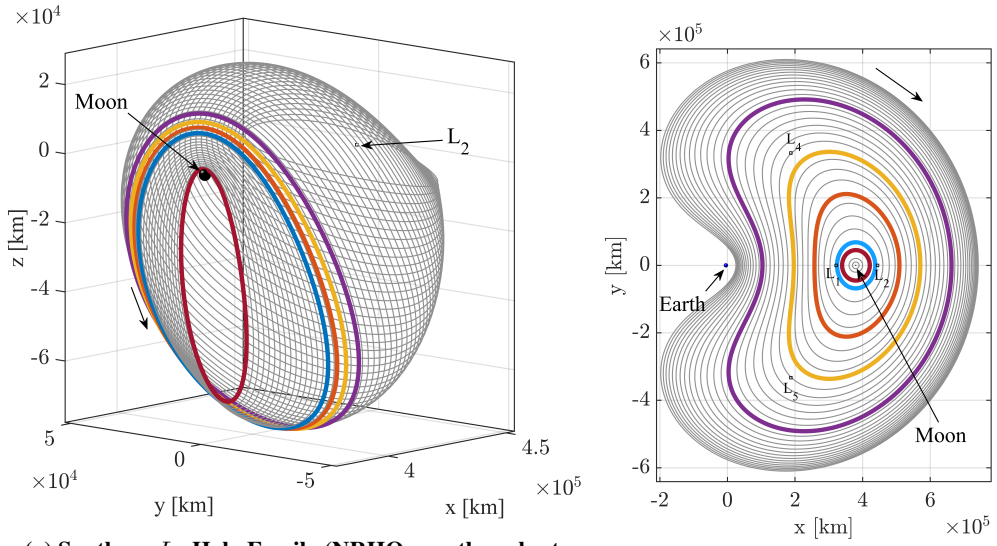

(a) Southern L_2 Halo Family (NRHOs are the subset between the maroon and purple highlighted orbits[8])

(b) DRO Family

Figure 1: Periodic Orbits of Interest Computed in the Circular Restricted Three-Body Problem and Plotted in Earth-Moon Rotating Frame.

Goals for a number of current mission scenarios have recently motivated investigations into designs for both low-thrust and impulsive transfers into and out of the L_2 NRHOs, in particular. In 2017, McGuire et al. examined a strategy to produce transfers into NRHOs and between cislunar multi-body orbits with a 40kW low-thrust engine using a trajectory design and optimization tool.[9] McCarty and McGuire utilized parallel monotonic basin hopping to mass-optimize a low-thrust NRHO to DRO transfer.[10] Also in 2017, Lantoine produced efficient impulsive NRHO to DRO transfers using a scheme that blends Earth-Moon-Sun ephemeris departure and arrival segments with a Moon-to-Moon transfer arc modeled in the Sun-Earth Circular Restricted Three-Body Problem (CR3BP).[11] These previous solutions, among others, illuminate the necessity for understanding complex behaviors in the NRHO neighborhood to more effectively design transfers in this regime. Therefore, rather than focusing solely on a mass- or time-optimized point solutions derived from an extensive grid search, further exploration of the dynamical structures in the region may offer a dynamical framework to alternatively initiate the design process. Potential transfer pathways are then constructed by combining arcs from various types of periodic orbits within the Earth-Moon system and, if applicable, their manifold structures, using an impulsive engine model. The goal of this investigation is design flexibility as well as predictable, intentional solution geometries, allowing for a wider exploration of available motions, contingencies in response to mission requirement modifications, and transfer solutions rooted in well-understood characteristic behaviors.

DYNAMICAL MODEL

The CR3BP serves as a reasonable approximation to higher-fidelity dynamical models in the Earth-Moon system while offering simplifications that allow for more straightforward concept development. Within this application of the CR3BP, the motion of a massless spacecraft under the gravitational influence of two primary bodies, P_1, the Earth, and P_2, the Moon, is considered. These two primary bodies, modeled as point masses, are assumed to move in circular orbits about

their common barycenter, B. The motion of the spacecraft is then described relative to a coordinate frame, $\hat{x}$-$\hat{y}$-$\hat{z}$, that rotates with the motion of the Earth and Moon. In this frame, the location of the spacecraft is described by the vector $\bar{r}_{B-s/c}$, originating at the barycenter, and is defined by the coordinates (x, y, z). By convention, quantities in the CR3BP are nondimensionalized such that the Earth-Moon distance, as well as the mean motion of the primaries, are both equal to a constant value of unity. As a consequence of the nondimensionalization, the distances from the Earth and Moon to the barycenter are represented as μ and $1-\mu$, respectively, where the parameter μ equals the ratio of the mass of the Moon to the total mass of the system; in this case, $\mu = 0.01215$. Within the context of the rotating frame, the scalar equations of motion for the spacecraft are

$$\ddot{x} - 2\dot{y} = \frac{\partial U}{\partial x},\ \ddot{y} + 2\dot{x} = \frac{\partial U}{\partial y},\ \ddot{z} = \frac{\partial U}{\partial z} \tag{1}$$

where the pseudo-potential function, $U = \frac{1}{2}(x^2+y^2) + \frac{1-\mu}{d} + \frac{\mu}{r}$, while $d = \sqrt{(x+\mu)^2 + y^2 + z^2}$, and $r = \sqrt{(x-1+\mu)^2 + y^2 + z^2}$. The CR3BP possesses one integral of the motion, denoted the Jacobi constant, JC, where $JC = 2U - v^2$, and v is the magnitude of the spacecraft velocity expressed in the rotating frame. The Jacobi constant is an energy-like parameter (constant along a ballistic arc) that offers clues to the available behavior, e.g., a larger Jacobi constant is indicative of a smaller orbital energy, therefore, the available motion is more limited. Across a family of periodic orbits, natural quantities that characterize the family, e.g., Jacobi constant and period, evolve smoothly. In Figure 2, curves, or hodographs, for Jacobi constant versus period are plotted for both the L_2 halo orbits and the DROs. Note, the NRHO region along the curve in Figure 2(a) is denoted by the region between the maroon and purple stars.

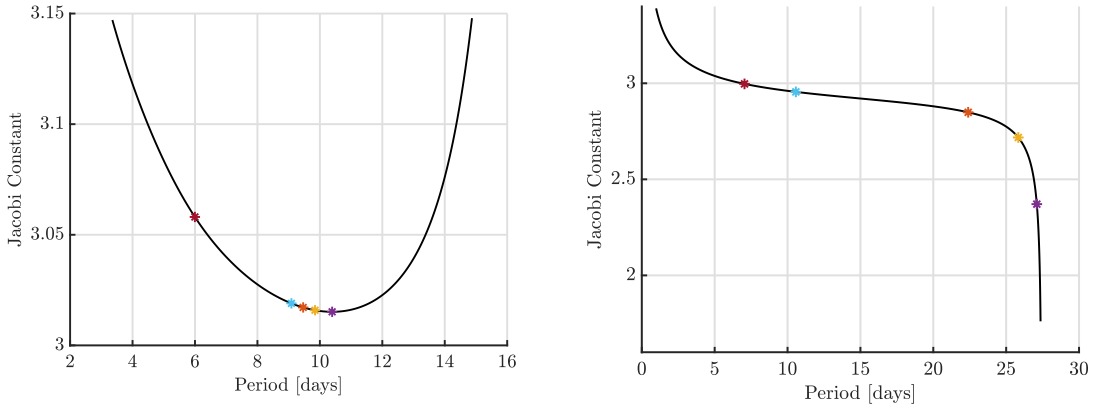

(a) L_2 Halo Orbit Family Hodograph

(b) DRO Family Hodograph

Figure 2: Jacobi Constant vs Period for the NRHOs and DROs.

NEARBY DYNAMICAL STRUCTURES

Orbital Stability and Bifurcations

Often leveraged to generate initial guesses, manifolds offer pathways for arrival at and departure from unstable periodic orbits. One of the challenges associated with transferring to/from NRHOs and DROs (as well as other stable or nearly-stable periodic orbits) is their lack of useful manifold

structures or arrivals/departures that evolve too slowly for practical application.[12,13] As an example, NRHO manifold structures are either poorly defined, as is the case near perilune,[14] or remain in the nearby vicinity for too many revolutions to guarantee the safety of assets left behind. Stability indices, defined as

$$\nu_i = \frac{1}{2}\left(||\lambda_i|| + \frac{1}{||\lambda_i||}\right), \tag{2}$$

offer insight into the orbital stability; in Equation (2), λ_i are the eigenvalues of the monodromy matrix, $\Phi(t+P,t)$, and P is the orbital period of the given orbit. Note that the eigenvalues of the monodromy matrix occur as two sets of reciprocal pairs and two trivial eigenvalues equal to unity, i.e., the set of eigenvalues from the monodromy matrix for a particular periodic orbit occur in the form: $(1, 1, \lambda_1, 1/\lambda_1, \lambda_2, 1/\lambda_2)$.[13] If all of the stability indices are equal to unity, an orbit is linearly stable and possesses no unstable subspace; if any nontrivial stability index has magnitude greater than unity, the orbit is unstable and natural flow exists into and out of the orbit. The magnitude of the stability index is directly related to the rate of departing/arriving flow.[12] Figure 3 illustrates the stability indices corresponding to the NRHOs (between the maroon and purple stars in Figure 3(a)) and the DROs as a function of perilune radius. As demonstrated by the magnitude of the stability indices for these orbits, natural flow into and out of these orbits is either nonexistent or too slow to offer utility for transfer design.

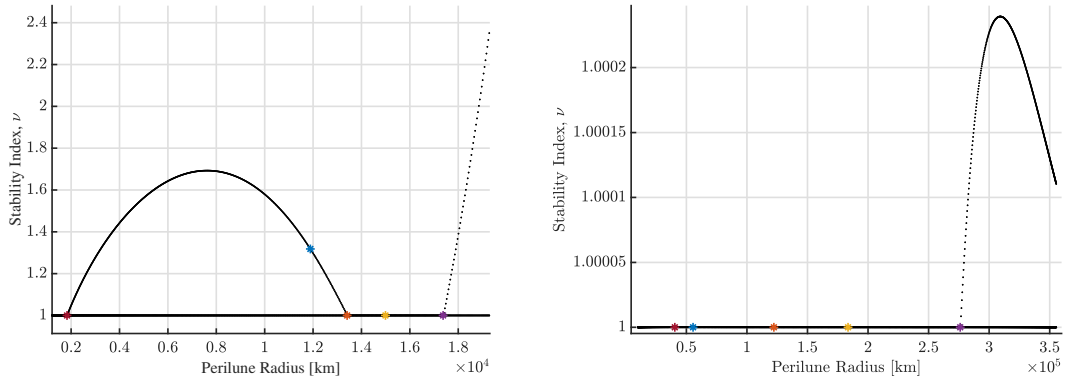

(a) NRHO Stabilty Indices **(b) DRO Stability Indices**

Figure 3: Stability indices for the L_2 NRHOs and the DROs demonstrating that these orbits are stable or nearly-stable.

Despite a lack of manifold structures that can be leveraged, other strategies for design of transfers into/out of the NRHOs and DROs are available. Maneuvers along the orbit paired with an optimization scheme can produce options, however, this method can result in unpredictable solution geometries and narrow basins of convergence. Alternatively, unstable structures that exist nearby the original orbit, in both energy and geometry, may be available for departing and arriving the vicinity. To identify nearby periodic orbit families that may offer useful flows, an examination of nearby structures that exist in the vicinity of the orbit of interest is a logical next step; the framework for this investigation is based on the identification and exploration of bifurcations in the region. Multiple types of bifurcations are available; monitoring the eigenvalues of the monodromy matrix and stability indices offers insight into the bifurcation types. Considered in this investigation are the following bifurcation types:

1. **Tangent Bifurcation:** As a general rule, a transition in stability characteristics along an orbit family denotes a bifurcation (as noted by changes in the value of the stability index). In the case of a change in family stability occurring simultaneously with two nontrivial eigenvalues of the monodromy matrix going to unity, $\lambda_j = \lambda_k = +1$, a tangent bifurcation (further delineated as either a cyclic fold, pitchfork bifurcation, or transcritical bifurcation) has occurred.[15]

2. **Period-Multiplying Bifurcations:** Period-multiplying bifurcations can occur without a change in orbital stability. As an example, when two nontrivial eigenvalues of the monodromy matrix, $\lambda_j = \lambda_k = -1$, a period-doubling bifurcation occurs. A period-multiplying bifurcation (of multiplying factor m) occurs when two nontrivial monodromy matrix eigenvalues occur at $\lambda_j, \lambda_k = \cos(2\pi/m) \pm i\sin(2\pi/m)$.[15]

3. **Secondary Hopf and Modified Secondary Hopf Bifurcations:** A less typical type of bifurcation is described as a secondary Hopf bifurcation; this type occurs when the eigenvalues depart the unit circle into the complex plane at a location other than at ± 1 along the real axis (therefore, a change in stability also occurs). A modified secondary Hopf bifurcation occurs when the eigenvalues depart the real line into the complex plane, however, this does not occur with a change in stability. In the special case of a secondary Hopf bifurcation (modified or regular), the eigenvalues are complex but with magnitude greater than unity indicating the existence of spiral manifolds (oscillatory and departing/approaching flow).[16]

In all mentioned bifurcations, other than the cyclic fold type, a new family of periodic orbits intersects with the current family; it is in this new family, which possesses members nearby in both energy and geometry, that useful unstable structures may arise.

In 1969, Broucke introduced an alternative method to identify bifurcations based on changes in the eigenstructure of the monodromy matrix.[17] In this technique, the nontrivial eigenvalues of the monodromy matrix for each family member are recast in terms of two parameters, α and β:

$$\alpha = -\left(\lambda_1 + \frac{1}{\lambda_1} + \lambda_2 + \frac{1}{\lambda_2}\right) = 2 - Tr\left(\Phi(t+P,t)\right) \tag{3}$$

$$\beta = \frac{1}{2}\left(\alpha^2 - \left(\lambda_1^2 + \frac{1}{\lambda_1^2} + \lambda_2^2 + \frac{1}{\lambda_2^2}\right)\right) = \frac{1}{2}\left(\alpha^2 + 2 - Tr\left(\Phi(t+P,t)^2\right)\right). \tag{4}$$

The scalars α and β fully define the set of four nontrivial eigenvalues, thereby reducing the set of parameters to be monitored from four to two. Additionally, using α and β to detect bifurcations eliminates the need to compute eigenvalues, thereby reducing numerical inaccuracies and computation time. The set $(\alpha,\ \beta)$ is plotted for each member of a family of periodic orbits on a Broucke stability diagram resulting in a curve that illustrates the evolution of the eigenstructure across the family.[16,18] The Broucke stability diagram in Figure 4 offers insight into the eigenvalue configuration in the complex plane. In this figure, the small graphic in each region illustrates the unit circle and the general arrangement of the four nontrivial eigenvalues. By noting changes in the eigenstructure over the evolution of the family based solely on the values of $(\alpha,\ \beta)$, bifurcations are detected. Bifurcations of interest (and their relation to the Broucke stability diagram) are described in Table 1.

Applications

In Figure 5, curves are plotted on the Broucke stability diagrams that correspond to the L_2 halo family (particularly the NRHO region) and the DRO family, with arrows indicating the direction

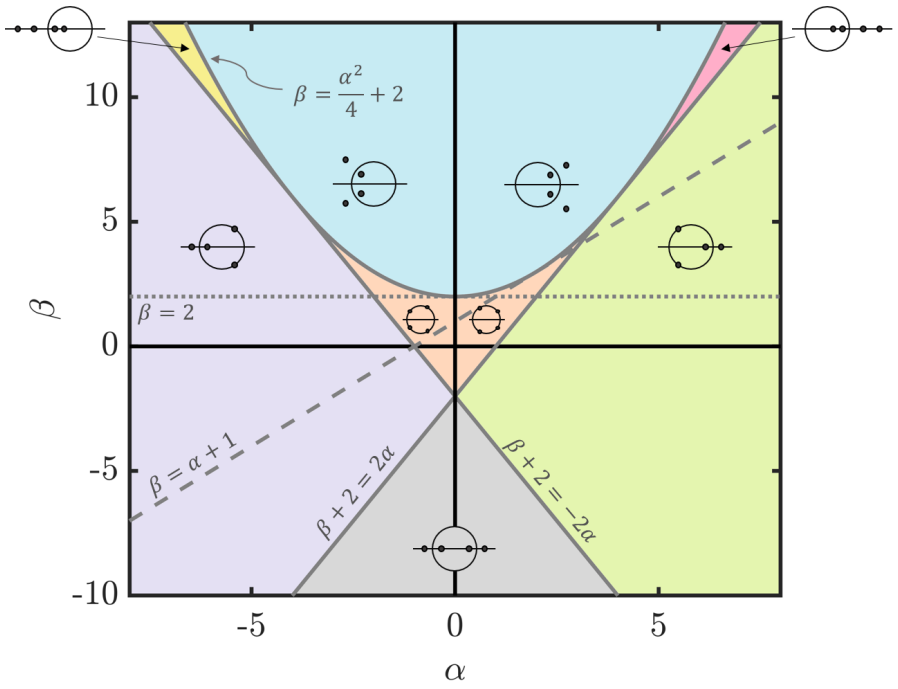

Figure 4: Broucke Stability Diagram.[17]

Table 1: Classification of bifurcations of interest based on a Broucke stability diagram.

Bifurcation Type	**Eqn. of Line Crossed**	**Color Transitions**	**Stab. Change?**
Tangent	$\beta + 2 = -2\alpha$	Orange $\leftrightarrow$ Purple Green $\leftrightarrow$ Grey Yellow $\leftrightarrow$ Purple	Yes
Period-Doubling	$\beta + 2 = 2\alpha$	Orange $\leftrightarrow$ Green Purple $\leftrightarrow$ Grey Pink $\leftrightarrow$ Green	Yes
Period-Tripling	$\beta = \alpha + 1$	N/A	No
Period-Quadrupling	$\beta = 2$	N/A	No
Secondary Hopf	$\beta = \frac{\alpha^2}{4} + 2$ $\alpha \in (-4, 4)$	Orange $\leftrightarrow$ Blue	Yes
Modified Secondary Hopf	$\beta = \frac{\alpha^2}{4} + 2$ $\alpha \in (-\infty, -4] \bigcup [4, \infty)$	Pink $\leftrightarrow$ Blue Yellow $\leftrightarrow$ Blue	No

of increasing perilune radius. In these figures, colored asterisks (*) indicate family members that correspond to bifurcations. Additionally, asterisks of the same color mark these family members in Figures 2 and 3; the orbits are also traced in the corresponding colors in Figure 1. To easily recognize these bifurcating orbits and the corresponding families to which they belong, a naming convention for these new families is necessary. For period-multiplying bifurcations (and the resulting higher-period families) the naming format is defined: 'Pm[originating family]$_n$', where 'Pm' refers to the order of the period-multiplication (e.g., period-doubling is reflected in m = 2), '[originating family]' refers to the family from which the bifurcating family has evolved (e.g., 'HO' refers to

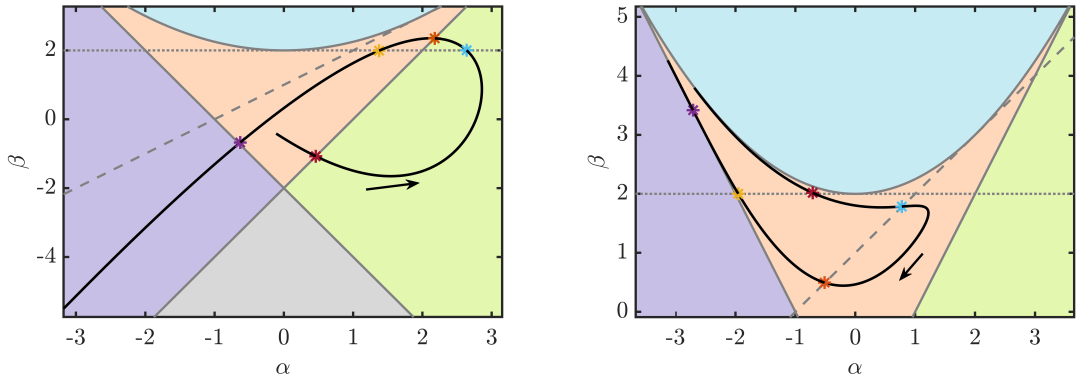

(a) L_2 NRHO Broucke Stability Diagram **(b) DRO Broucke Stability Diagram**

Figure 5: Broucke stability diagrams with a black curve representing periodic orbit family evolution; an arrow indicates the direction of increasing perilune radius.

halo orbits and 'DRO' refers to distant retrograde orbits), and 'n' denotes a sub-family identifier (i.e., for multiple bifurcations of the same type, the first family, in order of increasing perilune radius, is labelled n = 1, the second family is labelled n = 2, etc.). New families that originate from tangent bifurcations or Hopf bifurcations are named in accordance with a unique characteristic of the family and the 'n' sub-family identifier is maintained if necessary. The bifurcations (and the bifurcating families) across the NRHO region, as well as the DRO family, in order of increasing perilune radius, are delineated in Tables 2 and 3, respectively.

Table 2: Bifurcations across the NRHO region in the halo family and the corresponding new orbit families in order of increasing perilune radius.

Color	Bifurcation Type	Name of New Family	Other Useful Information
Maroon	Period-Doubling	$P2HO_1$	Also known as the butterfly family.
Blue	Period-Quadrupling	$P4HO_1$	
Orange	Period-Doubling	$P2HO_2$	
Gold	Period-Quadrupling	$P4HO_2$	
Purple	Tangent (Cyclic Fold)	N/A	No new family originates at a cyclic fold bifurcation.

Table 3: Bifurcations across the DRO family and the corresponding new orbit families in order of increasing perilune radius.

Color	Type	Name of New Family	Other Useful Information
Maroon	Period-Quadrupling	$P4DRO_1$	
Blue	Period-Tripling	$P3DRO_1$	Only one period-three DRO family exists (denoted the P3DRO family).
Orange	Period-Tripling	$P3DRO_2$	
Gold	Period-Quadrupling	$P4DRO_2$	
Purple	Tangent	3D-DRO	A three-dimensional family of DROs.

Employing a multiple-shooting pseudo-arclength continuation scheme, the new families of periodic orbits originating at each of these bifurcations are computed. In Figures 6 through 9, the

families originating from the NRHO bifurcations are plotted (and colored by Jacobi constant) along with the stability index values versus orbital period. Note that in each example, the southern orbits (or the segment of the family that possesses a majority of motion in the negative z-direction) are plotted. In each case, a northern analog also exists.

A range of orbits in the $P2HO_1$ family is plotted in Figure 6. This family, often termed the butterfly family, is characterized by two lobes in a "figure-8" shape, one on the L_1 side of the Moon and one on the L_2 side;[12] a distinct advantage for periodic orbits in this family is the ability to access both sides of the Moon using natural ballistic motion. Note that the loop structures that appear in Figure 6(a) represent Hopf bifurcations. The $P4HO_1$ family is plotted in Figure 7. Note that, at

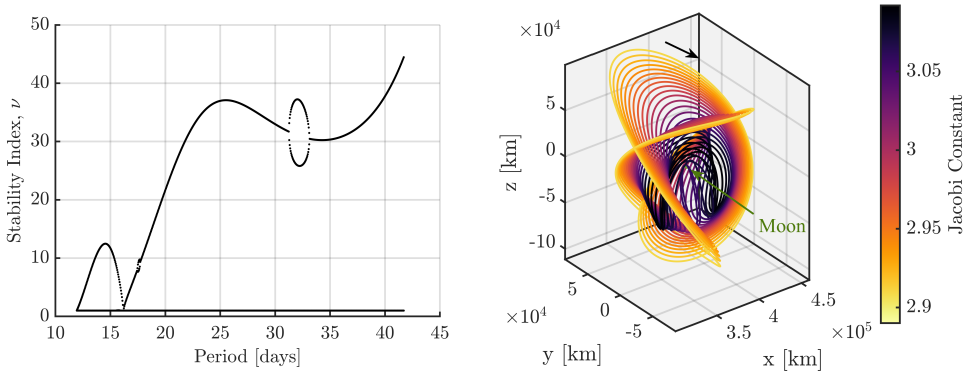

Figure 6: $P2HO_1$ (Butterfly) Family.

the furthest extent of the family in Figure 7(b) there are multiple passes inside the lunar radius. However, orbits in this family may offer the ability to adjust the orbital plane using natural motion as some lobes exist in the yz-plane while others are approaching a more planar-type motion. Next, Figure 8 illustrates the characteristics of orbits in the $P2HO_2$ family. In contrast to the other

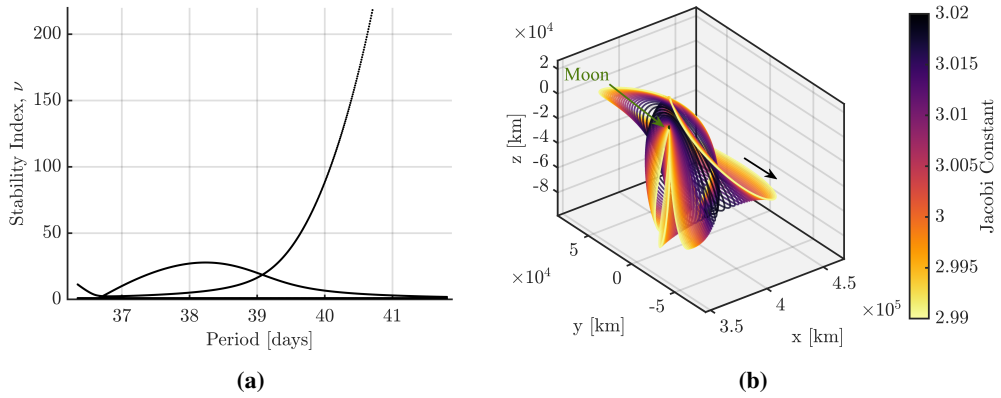

Figure 7: $P4HO_1$ Family.

higher-period families that bifurcate from the NRHO region, this family continues smoothly into its northern counterpart passing through the xy-plane (similar to northern and southern halo orbit families). Although the $P2HO_2$ orbits posses periods approximately double the period of the NRHOs,

the P2HO$_2$ family does not offer access to both the L_1 and L_2 sides of the Moon as do members of the P2HO$_1$ family; rather, the P2HO$_2$ orbits offer access in an "East-West" type motion–which may offer utility in certain scenarios. Finally, a portion of the P4HO$_2$ family of orbits is plotted in Figure

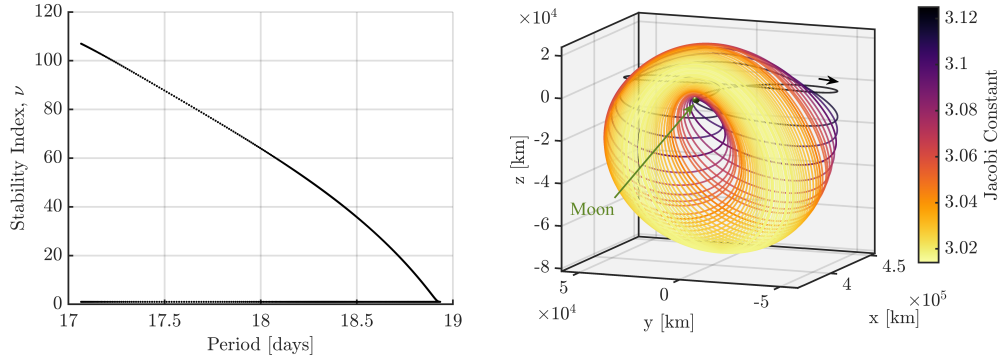

(a) **(b)**

Figure 8: P2HO$_2$ Family.

9. The extent of this family is quite large and extends well beyond the range in Figure 9(b). While some of the larger members of this family offer exotic motion that is both perpendicular to and within the orbital plane (not pictured here) smaller members more closely approximate NRHO-like motion, albeit, periodic with four lunar passes instead of one.

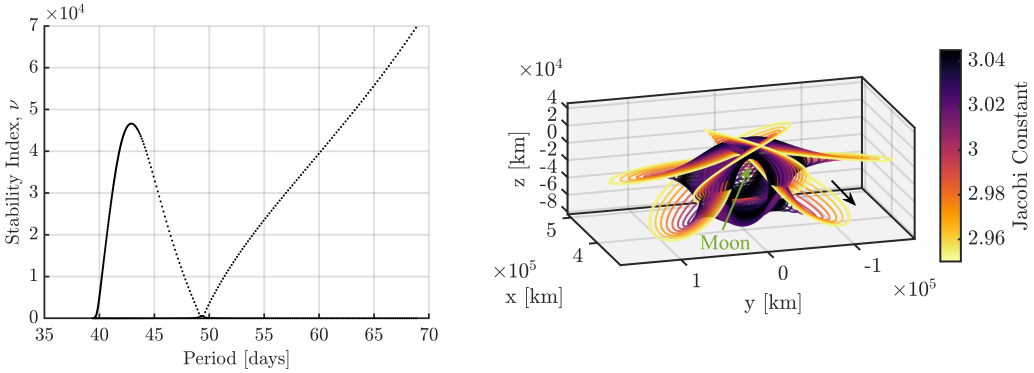

(a) **(b)**

Figure 9: P4HO$_2$ Family.

In Figure 10, a member from each of these new families is plotted in the Earth-Moon rotating frame to illustrate their complex multi-revolution geometry and to better illustrate their unique and distinct characteristics. In each plot, the Moon appears as a grey sphere and the direction of motion along the trajectory is indicated by a black arrow. Two distinct perilune radii exist for the P4HO$_1$, P2HO$_2$, and P4HO$_2$. In the P2HO$_1$ trajectory, there are two perilune passages, but both occur at the same altitude. The magnitude of the stability index across each of the higher-period halo orbit families indicates that departure/arrival along an unstable/stable manifold is more rapid than the equivalent departure/arrival along an NRHO manifold. Since it is likely that an asset will remain in

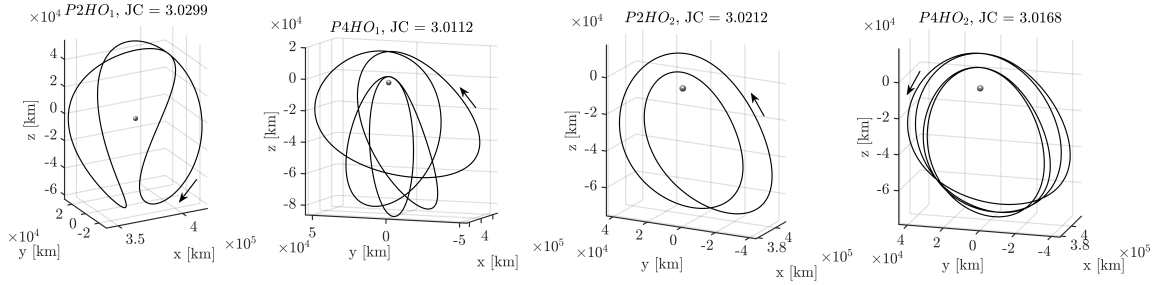

Figure 10: Select Members from Each of the Higher-Period Families that Bifurcate from the NRHOs.

an NRHO, a departure that requires fewer revolutions to depart is desirable as it lessens the chances for an impact. Leveraging any structures (or orbits) that may exist in the vicinity with smaller time constants can be beneficial. Additionally, since there are likely to be time-of-flight limitations, short transfer times are desirable.

A similar characterization for the DRO family is plotted in Figure 1(b). The DROs are attractive for long-duration missions due to their inherent stability and a potential for low orbit maintenance costs. Due to the lack of an unstable subspace, however, arriving to/departing from orbits in this family poses challenges. Families that originate from the DRO bifurcations, colored by Jacobi constant, are plotted in Figures 11 to 14 along with plots of stability index versus orbital period. Both the $P4DRO_1$ family and the 3D-DRO family (plotted in Figures 11(b) and 14(b), respectively) are stable or nearly-stable, similar to the foundational DRO family. Thus, these orbits may not offer useful initial guesses for transfer options, however, they may offer long-term, low stationkeeping cost destinations for future Gateway mission scenarios. In contrast, the P3DRO and the $P4DRO_2$ families each possess members with manifold structures that can be accessed for initial guesses in transfer design. In fact, manifolds originating from a P3DRO are employed for initial guess generation to produce transfers into a DRO from an NRHO by Zimovan et al. in 2017.[12] As noted

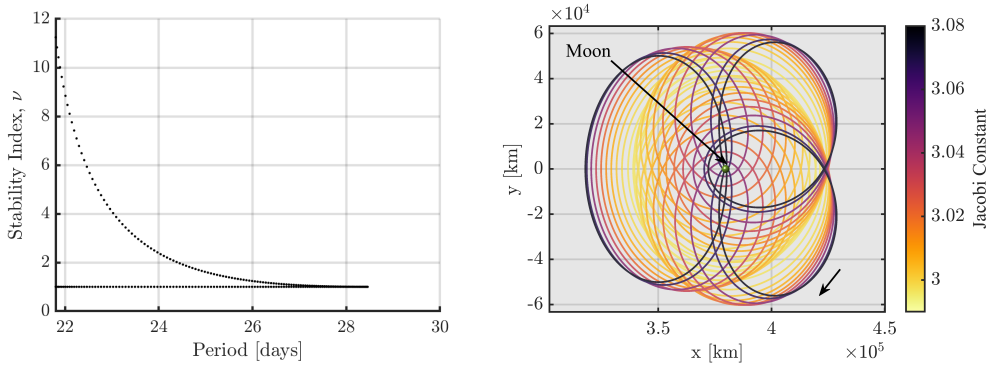

Figure 11: $P4DRO_1$ Family.

in Table 3, only one P3DRO family exists despite the fact that there are two bifurcations along the DRO family (colored in blue and orange in Figure 1(b)), i.e., two periodic orbits belong to both the DRO family and the P3DRO family.

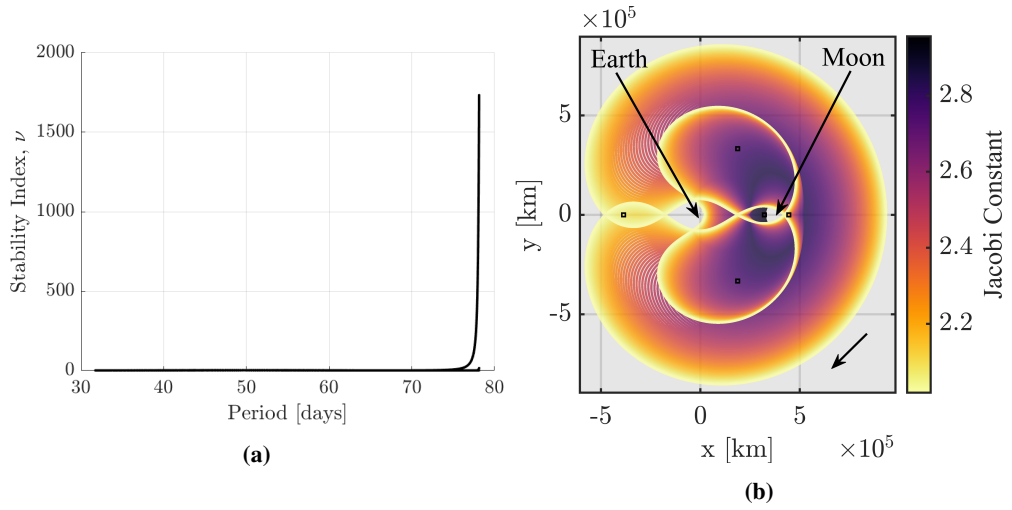

Figure 12: P3DRO Family.

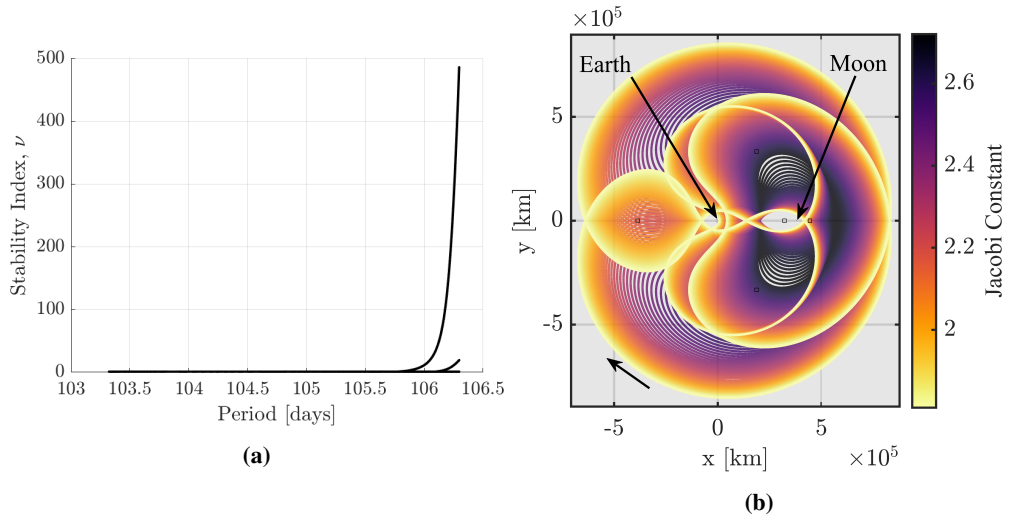

Figure 13: P4DRO$_2$ Family.

Excursions throughout the Earth-Moon neighborhood, even to the vicinity of the Lagrange points L_3, L_4, and L_5, are available via some of the larger members of the P3DRO and P4DRO$_2$ families; although not the focus of this investigation, moving from a DRO to other destinations in these vicinities may be an option through these higher-period orbits and their manifolds. As a final note, the 3D-DROs offers potential eclipse avoidance properties due to the out-of-plane characteristics; given the stable nature of these 3D trajectories, it is likely that orbit maintenance costs in this vicinity are minimal. Figure 15 illustrates a member from each of the bifurcating families that originate from the DROs. Note that the primary direction of motion is retrograde.

Some of the structures exemplified by the nearby bifurcating families are apparent in plots of transfer trajectories from NRHOs to DROs and other destinations that have been generated by other authors. In McCarty et al., a 9:2 NRHO to DRO transfer features a geometry post-NRHO departure that shares characteristics with a P2HO$_2$ orbit. This particular transfer also features motion

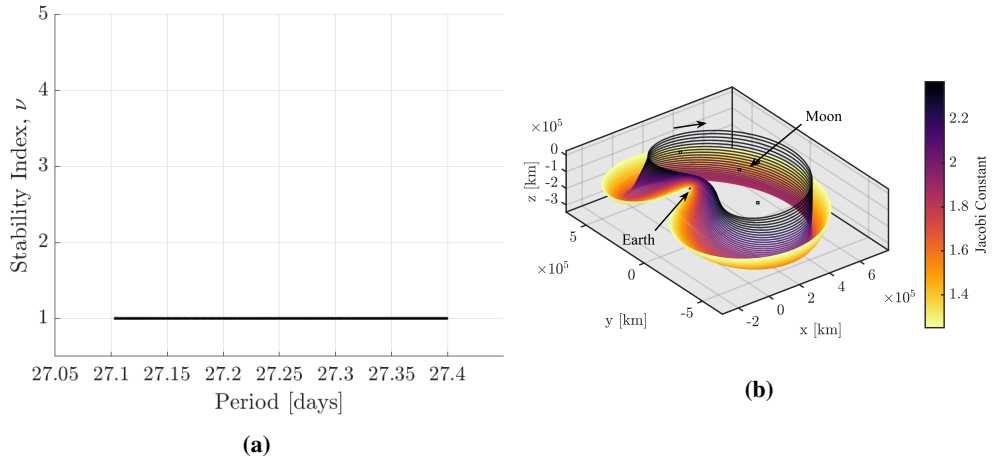

(a) (b)

Figure 14: 3D-DRO Family.

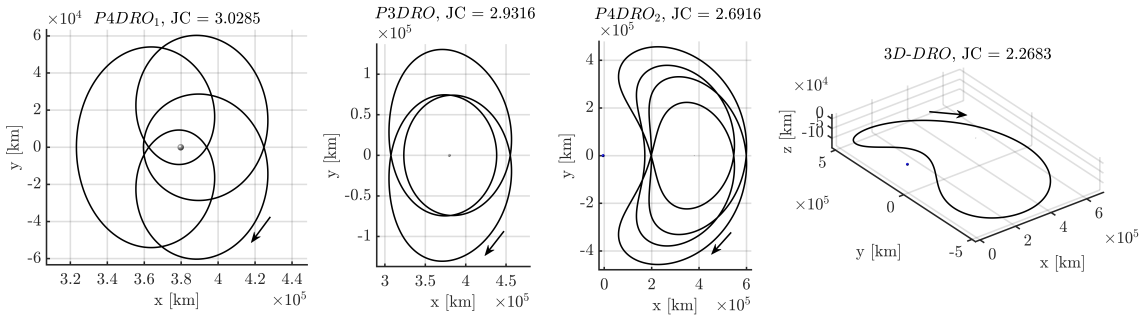

Figure 15: Select Members from Each of the Families that Bifurcate from the DROs.

consistent with either a P3DRO or P4DRO$_2$ near the arrival into the DRO.[10] Similarly, a presentation delivered to the NASA Advisory Council entitled *Gateway Update* depicts a low-thrust transfer from an NRHO to a DRO that appears to include structures from either a P2HO$_1$, P4HO$_1$, or P4HO$_2$ after departure from the NRHO.[19] Recognizing the local structures that may lead to optimal results could offer mission designers a more informed initial guess and an increased intuition in the design process for certain geometries. Additionally, nearby higher-period motion also offers insight into some of the motion that emerges during numerical convergence of the NRHOs in higher-fidelity models. As explored in Davis et al. and Zimovan et al., as perturbations from the Sun or other planetary bodies are included in the simulation, a drifting between various families that are nearby in Jacobi constant and geometry occurs–especially for the more unstable members.[12,20] Since nearby unstable dynamical structures appear to influence or offer insight into the natural flow in the vicinity of stable or nearly-stable orbits, they have the potential to supply trajectory designers with additional tools to aid in the transfer design process.

TRANSFER TRAJECTORIES DESIGN METHODOLOGY

Since interest in transfers between NRHOs and DROs is increasing, trajectories that link the 9:2 synodic resonant NRHO (the current Gateway baseline orbit) and a DRO at nearly the same Jacobi constant value are explored. To generate an initial guess for transfers in this vicinity, the higher-period families that bifurcate from the NRHOs, the manifolds that correspond to these orbits, and

a variety of well-known resonant and libration point orbits are included within the design database. The resonant and libration point orbits are extracted from the Adaptive Trajectory Design (ATD) catalog, designed as a part of a collaborative effort between Purdue University and NASA Goddard Space Flight Center.[21–24] To demonstrate that higher-period orbits (nearby in geometry and energy) offer useful initial guesses, it is necessary to first demonstrate that connections between the 9:2 NRHO and higher period orbits do indeed exist.

Transfers between orbits at the same energy level allow maneuvers to be used for geometry changes, rather than changes in Jacobi constant value. Therefore, in this investigation, the NRHO, DRO, and all intermediate orbits used to generate initial guesses are characterized by a Jacobi constant equal to that of the 9:2 NRHO ($JC = 3.047$). Figure 16 illustrates the higher period orbits that exist at this energy level. Clearly, due to both close proximity and a corresponding direction of motion along the orbits, transfers from the NRHO into the $P4HO_2$ and $P2HO_2$ orbits at the same energy level are easily accomplished. Transfers into the $P2HO_1$ orbit are also successfully accomplished, however, near apolune where the NRHO and L_2 lobe of the $P2HO_1$ orbit are nearby in position, the directions of motion are opposing, which must be accomodated. A multiple-shooting scheme that incorporates a stable manifold arc from the higher-period orbit as an initial guess is leveraged to generate direct impulsive transfer options from the NRHO. Since a demonstration of the utility of these higher-period orbits in designing transfers that originate at the NRHO is the main goal, feasible transfers that include two impulsive maneuvers are delivered. Low-cost, low time-of-flight motion between the NRHO and $P2HO_1$, $P4HO_2$ and $P2HO_2$ orbits at $JC \approx 3.047$ appears in Figure 17. A transfer between the NRHO and the $P4HO_1$ is not included since a $P4HO_1$ orbit does not exist at this energy level. In Figure 17, the numbered red circles indicate the impulsive maneuver locations along the transfer arc; in each sample transfer, a Δv is incorporated to both depart the NRHO and to enter into the higher-period orbit. The time-of-flight for each transfer depicted in Figure 17 is around 20 days and the maneuver total is on the order of 200 m/s.

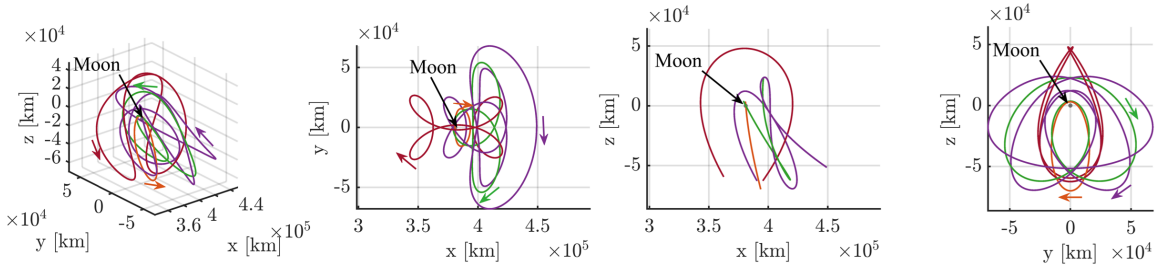

Figure 16: A 9:2 Synodic Resonant NRHO with Higher-Period Orbits that Occur at the Same Jacobi Constant ($JC \approx 3.047$) where Orange: NRHO, Red: $P2HO_1$, Green: $P2HO_2$, Purple: $P4HO_2$

As a next step, Poincaré maps are constructed to link manifold arcs from these higher-period orbits directly to a DRO or to other useful structures *en route* to a DRO. Two structures of particular interest are a planar 3:4 resonant orbit and a 4:3 resonant orbit (from the Orbit Reference Catalog[21–24]) due to the fact that they not only share similar characteristics with manifolds from each of the higher-period halo orbits but the resonant orbits also each possess retrograde loops around the Moon nearby the DRO of interest, as apparent in Figure 18. Selecting a hyperplane at $\{\Sigma : y = 0\}$, an x-v_y Poincaré map is generated that reflects a combination of the stable and unstable manifold crossings of the higher-period halo orbits, plane crossings from the periodic 3:4 and 4:3 resonant

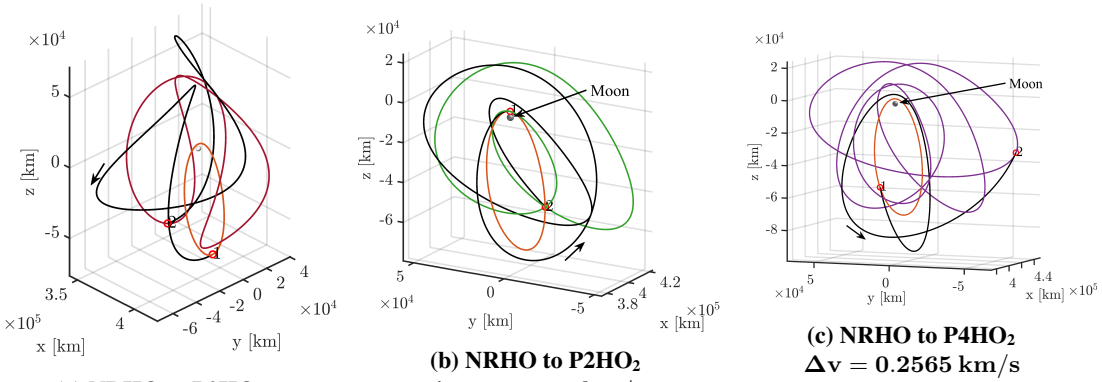

(a) NRHO to P2HO$_1$
$\Delta v = 0.2130$ km/s
TOF $= 21.48$ da

(b) NRHO to P2HO$_2$
$\Delta v = 0.2466$ km/s
TOF $= 21.25$ da

(c) NRHO to P4HO$_2$
$\Delta v = 0.2565$ km/s
TOF $= 16.36$ da

Figure 17: Transfers Between an NRHO and Higher-Period Orbits Plotted in the Earth-Moon Rotating Frame.

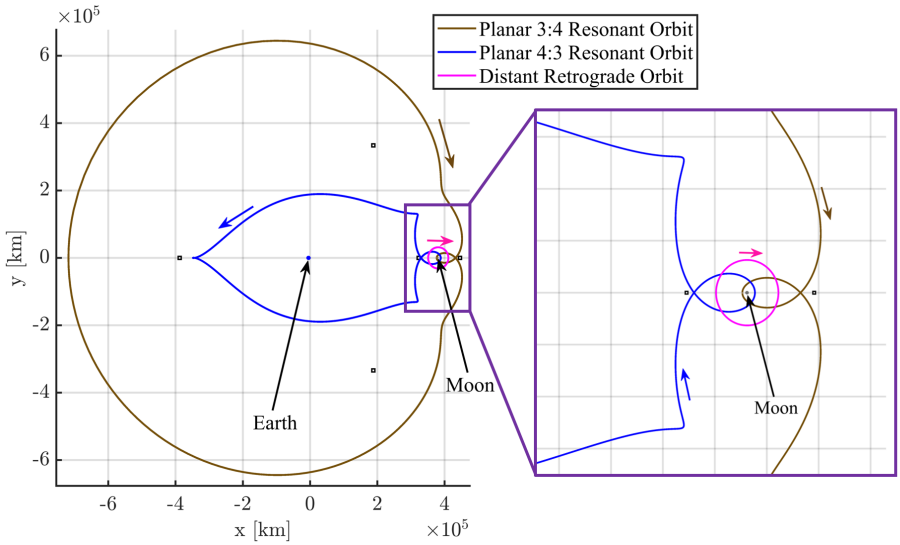

Figure 18: Useful Resonant Orbits and a DRO at $JC \approx 3.047$.

orbits, as well as the DRO plane crossings. A sample Poincaré map for creating a transfer from a P2HO$_2$ to a DRO via an arc originating from a 3:4 resonant orbit appears in Figure 19(a). In this map, triangles indicate periodic orbit crossings and circles highlight manifold crossings (red circles indicate unstable manifold crossings, while blue circles indicate stable manifold crossings). The center of each marker is colored according to the orbit from which it was generated; a green centered marker indicates origination at a P2HO$_2$ and a black centered marker denotes origination at a 3:4 resonant orbit. As a sample initial guess generated via the Poincaré map, the green arrow in Figure 19(a) is directed at a P2HO$_2$ unstable manifold crossing on the map, while the black arrow indicates a stable manifold crossing of the 3:4 resonant orbit. The trajectory arcs associated with these crossings are plotted in Figure 19(b), in red and blue, respectively, along with the periodic orbits from which they are generated; these manifold arcs form the basis for an initial guess to

produce a transfer linking the P2HO$_2$ and DRO.

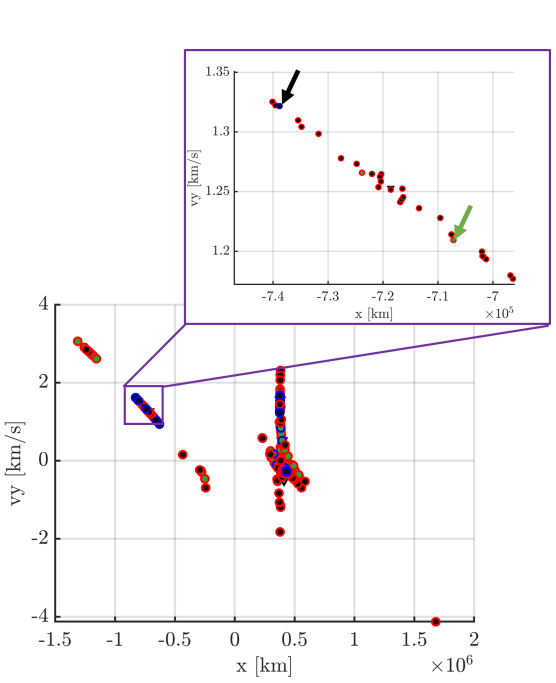

(a) Poincaré map that includes manifold crossings from the P2HO$_2$ and 3:4 resonant orbit

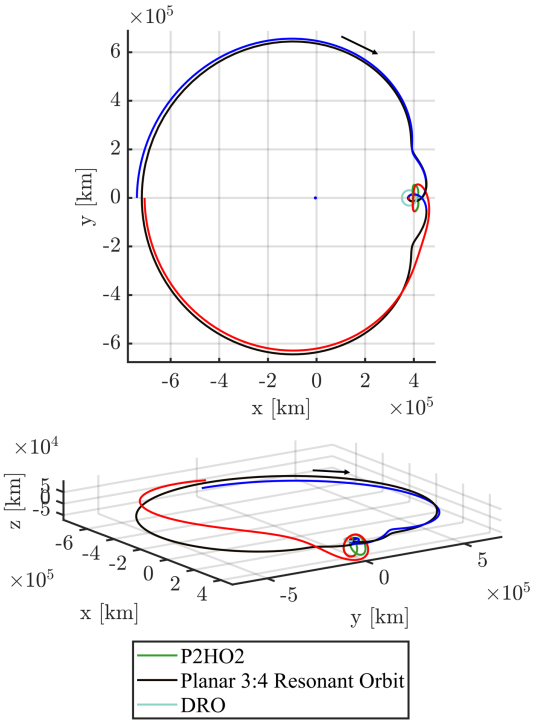

(b) Manifolds associated with the selected Poincaré map crossings in Figure 19(a)

Figure 19: A Poincaré map is used to select trajectory segments that serve as an initial guess in a targeting scheme.

To maintain the characteristics and geometry of an initial guess for a transfer trajectory, constructed through an intentional selection of orbit segments, a minimum norm multiple shooting scheme is used to enforce constraints and produce a converged solution. A variety of transfer geometries that exist between the higher period halo orbits and a DRO are illustrated in Figures 20 through 22. In each transfer, a similar strategy is employed to generate the initial guess for the corrections scheme, that is, one consistent with the technique in Figure 19. Note that the converged transfer solution for the initial guess illustrated in Figure 19(b) is plotted in Figure 20(a). The final solution includes three maneuvers: one to depart the P2HO$_2$, one on the L_3 side of Earth (to accomplish the majority of the plane change), and one to enter the DRO. The total time-of-flight (TOF) is 89.16 days and the total Δv is $0.5969\ km/s$. The transfer plotted in Figure 20(b) requires a similar total propellant cost (requiring a total Δv of $0.5595\ km/s$ across three maneuvers) while requiring a total time-of-flight of 80.67 days. In this example, a manifold from the P2HO$_2$ is combined with a manifold from a planar 4:3 resonant orbit; the corrections process shifts the arc from the 4:3 resonant orbit out-of-plane, however, the resonant geometry is still apparent.

Manifolds originating from a P4HO$_2$ family member offer multiple geometries that allow for transfers into the DRO as well. In Figure 21(a), a manifold from the P4HO$_2$ orbit supplies an initial guess for a direct connection into the DRO. The solution requires two maneuvers and a total cost of $\Delta v = 0.4859\ km/s$ over a TOF of 40.69 days. Figure 21(b) includes a transfer from the

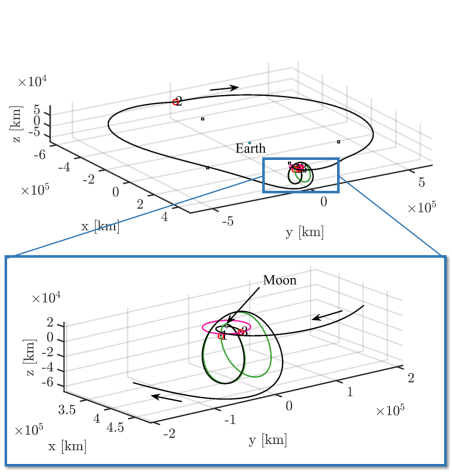

(a) P2HO$_2$ to DRO (via a 3:4 Resonant Orbit)
$\mathbf{\Delta v = 0.5969\ km/s}$
$\mathbf{TOF = 89.16\ da}$

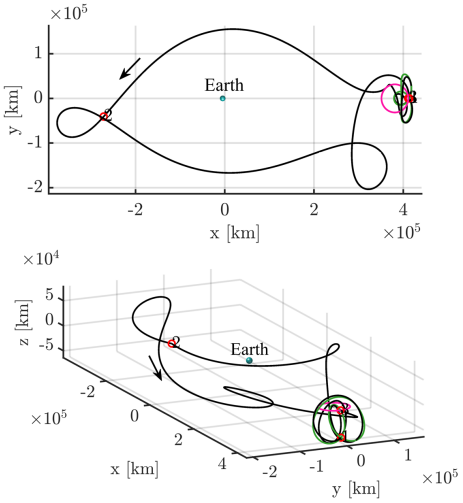

(b) P2HO$_2$ to DRO (via a 4:3 Resonant Orbit)
$\mathbf{\Delta v = 0.5595\ km/s}$
$\mathbf{TOF = 80.67\ da}$

Figure 20: Transfers between a P2HO$_2$ and a DRO Plotted in the Earth-Moon Rotating Frame.

P4HO$_2$ to the DRO using an intermediate arc from a 3:4 resonant orbit for the initial guess; this transfer requires $\Delta v = 0.6341\ km/s$ with three maneuvers over 81.67 days. Note that the majority of the plane change is accomplished via a ballistic arc departing from the vicinity of the P4HO$_2$ after the first maneuver–the unstable manifold supplied in the initial guess delivered much of the required plane change to move from the NRHO to the DRO. An alternative geometry is apparent in Figure 21(c). In this transfer, a 4:3 resonant orbit arc provides the initial guess. Similar to the transfer in Figure 20(b), the final solution moves the planar initial guess out-of-plane, however, the general geometry is maintained. The converged transfer incurs a 75.05 day TOF with a total cost of $\Delta v = 0.7613\ km/s$.

As previously investigated by Pritchett, Zimovan, and Howell, the P2HO$_1$ orbits, also known as butterfly orbits, offer segments for transfer initial guesses between the NRHO and DRO.[25] Important to note, however, are that the manifolds originating from certain P2HO$_1$ orbits are *spiral* modes, meaning that they spiral around the orbit while departing/arriving. These orbits possess complex eigenvalues with magnitudes greater than one. Figure 22 illustrates a case where an unstable manifold from a P2HO$_1$ is connected to a segment from a 4:3 resonant orbit to form a transfer initial guess. The solution possesses three maneuvers with a total Δv of $0.4961\ km/s$. The transfer time of flight is 97.41 days.

The solutions in Figures 20 - 22 serve as a representative sub-sample of available transfer geometries that exist between the higher-period halo orbits and the selected DRO. Incorporating higher-period DRO manifolds may offer significant insight into arrival geometries that naturally flow into the region. Without any optimization, reasonable times of flights and propellant costs for predictable solution geometries emerge that maintain the characteristics of the initial guess. Combining a transfer from an NRHO to a higher-period orbit (e.g., one from Figure 17) with a transfer from the higher-period orbit to a DRO (e.g., those in Figures 20 - 22) supplies a converged solution linking

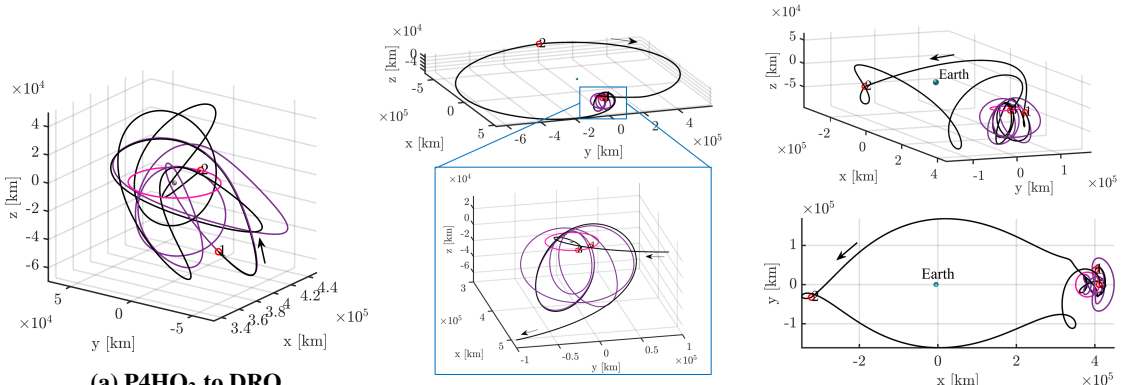

(a) P4HO$_2$ to DRO
$\mathbf{\Delta v = 0.4859\ km/s}$
$\mathbf{TOF = 40.69\ da}$

(b) P4HO$_2$ to DRO (via 3:4 Resonant Orbit)
$\mathbf{\Delta v = 0.6341\ km/s}$
$\mathbf{TOF = 81.67\ da}$

(c) P4HO$_2$ to DRO (via 4:3 Resonant Orbit)
$\mathbf{\Delta v = 0.7613\ km/s}$
$\mathbf{TOF = 75.05\ da}$

Figure 21: Transfers Between a P4HO$_2$ and a DRO Plotted in the Earth-Moon Rotating Frame.

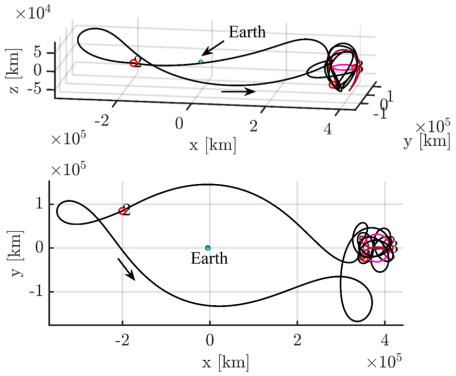

Figure 22: Transfer between a P2HO$_1$ and a DRO (via a 4:3 Resonant Orbit)
$\mathbf{\Delta v = 0.4961\ km/s}$
$\mathbf{TOF = 97.41\ da}$

an NRHO and a DRO; such solutions serve as starting points for optimization. Since it may not be necessary to transit through the higher period orbit *en route* to the DRO, transfer times may decrease and geometry may shift slightly within an optimization scheme. Alternatively, transit through the intermediate higher period orbit may be used for spacecraft phasing or for check-out procedures prior to departure along a second transfer arc that may depart far from the NRHO around the Earth-Moon system.

As an example of a two phase transfer in which the intermediate higher period orbit is included along the path, the transfer trajectory linking the NRHO and a P2HO$_2$, in Figure 17(b), and the transfer arc from that particular P2HO$_2$ to the DRO, in Figure 20(a), are optimized using MATLAB's "fmincon." The simple optimization scheme uses a combination of cost functions and built-in algorithms to produce reduced-cost transfers. First, the feasible guess (generated via a minimum norm differential corrections scheme) is optimized using an interior-point method with an objective of $\min J = \sum_i ||\Delta \mathbf{v}_i||^2$; in this cost function, $||\Delta \mathbf{v}_i||$ represents the maneuver magnitude at each

patch point, including the first patch point at departure and the final patch point corresponding to arrival at the destination. This objective function is selected due to its favorable conditioning and the existence of relatively simple partial derivatives. As a second step, the optimal result seeds a sequential quadratic programming optimization scheme with a cost function given as $\min \widetilde{J} = \sum_i ||\Delta \mathbf{v}_i||$. This second phase provides some additional reduction in cost and the objective function, $\widetilde{J}$, by minimizing the total transfer cost. (Note that minimizing J does not always equate to minimizing $\widetilde{J}$, however, a two-step optimization scheme is used due to numerical challenges within the formulation in $\widetilde{J}$.) For each of the two optimization steps, the departure and arrival positions along the initial periodic orbit and the final periodic orbit, respectively, are fixed to be equivalent to the locations given in the initial feasible solution. Additionally, the TOF along the transfer arcs is constrained to be equivalent to the TOF for the feasible solution. Finally, maneuvers are allowed at any patch point along the trajectory. The resulting optimized transfer geometries for both phases of the transfer between the NRHO and the DRO are plotted in Figure 23. Phase one of the transfer, a segment

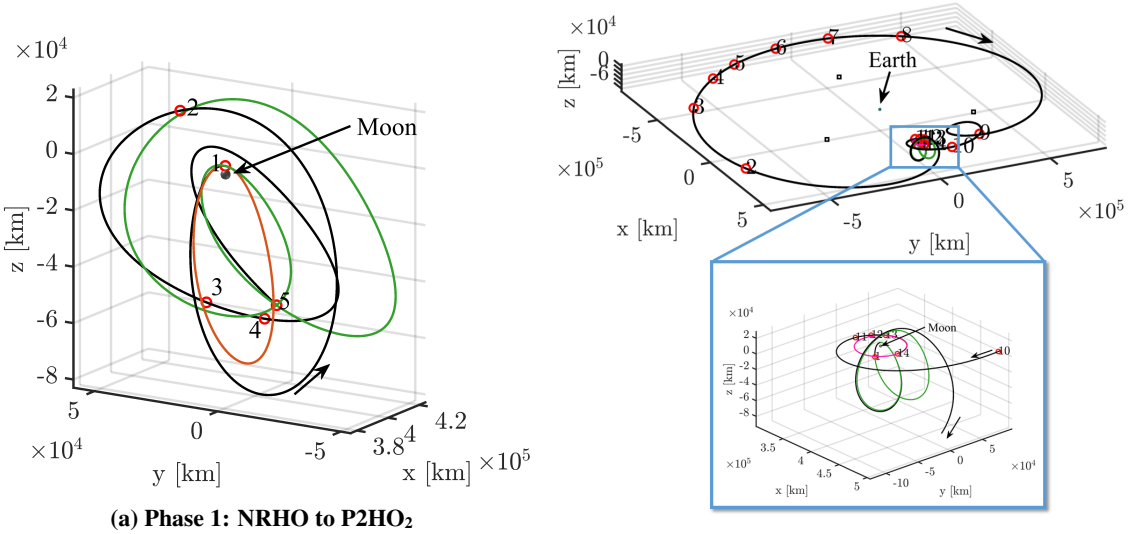

(a) Phase 1: NRHO to P2HO$_2$

(b) Phase 2: P2HO$_2$ to DRO

Figure 23: Optimized Transfer from an NRHO to a DRO via a P2HO$_2$. Maneuvers are numbered and marked as red circles.

connecting the NRHO to the P2HO$_2$, requires a total cost of $89.9\ m/s$ over four maneuvers. The geometry of the feasible solution (plotted in Figure 17(b)) is readily apparent in the reduced-cost result in Figure 23(a). The second phase of the transfer, plotted in Figure 23(b), links the P2HO$_2$ to a DRO. The total cost over fourteen maneuvers is $0.2156\ km/s$. Characteristics of the initial guess (plotted in Figure 19(b)) and the feasible solution (illustrated in Figure 20(a)) are maintained in this reduced-cost configuration. Using this result, a more complete optimization process, incorporating additional constraints and relaxing some of the requirements in this framework, may introduce additional options. The overall strategy–initial guesses for transfers based on known geometries and characteristic flow in the region, intermediate feasible transfers, and an optimization scheme–aims to deliver a predictable solution geometry and a flexible transfer design methodology to aid in moving throughout this complex regime.

CONCLUDING REMARKS

The NRHOs support NASA's Gateway objectives; to effectively operate in this complex multi-body dynamical regime, a better understanding of the motion in the vicinity is necessary. In this investigation, nearby structures that originate from bifurcations along the NRHO subset of the L_2 halo family are explored and their stability properties are characterized. Similarly, due to the fact that a DRO is a destination of interest for future operations, nearby structures bifurcating from the DRO family are explored as well. The motion characterized by these nearby orbit families offers insight into previously constructed transfer solutions and higher-fidelity motion in the vicinity of the NRHOs. A strategy to construct transfer trajectories between an NRHO and a DRO using higher-period orbits, their manifold structures, and other well-known orbits in the vicinity (e.g., resonant orbits) is summarized. As illustrated by the numerous nearby dynamical structures (both periodic orbits and manifolds belonging to unstable members of these families) motion in the vicinity of the NRHOs and DROs is complex and a better understanding of the fundamental motion in this regime offers a more informed design approach for transfers between these stable orbits that leads to design flexibility and predictable solution geometries.

ACKNOWLEDGMENTS

The authors wish to thank Kenza Boudad and Andrew Cox for the invaluable discussions and lines of inquiry during this investigation. Additionally, the authors wish to thank the Purdue University School of Aeronautics and Astronautics for the facilities and support, including access to the Rune and Barbara Eliasen Visualization Laboratory. This work was supported by a NASA Space Technology Research Fellowship, NASA Grant 80NSSC18K1153, as well as NASA Grant and Cooperative Agreement 80NSSC18M0122.

REFERENCES

[1] R. Whitley and R. Martinez, "Options for Staging Orbits in Cis-Lunar Space," *2016 IEEE Aerospace Conference*, 2016.

[2] W. H. Gerstenmaier, "Progress in Defining the Deep Space Gateway and Transport Plan," `https://www.nasa.gov/sites/default/files/atoms/files/nss_chart_v23.pdf`, March 28, 2017.

[3] "Deep Space Gateway to Open Opportunities for Distant Destinations," `https://www.nasa.gov/feature/deep-space-gateway-to-open-opportunities-for-distant-destinations`, August 24, 2018. Editor: Kathryn Hambleton.

[4] L. Capdevila, *A Transfer Network Linking Earth, Moon and the Libration Point Regions in the Earth-Moon System*. Ph.D. Dissertation, Purdue University, West Lafayette, Indiana, 2016.

[5] J. S. Parker, C. Bezrouk, and K. E. Davis, "Low-Energy Transfers to Distant Retrograde Orbits," *Advances in the Astronautical Sciences Spaceflight Mechanics 2015*, AAS 15–311.

[6] J. F. C. Herman, *Improved Collocation Methods to Optimize Low-Thrust, Low-Energy Transfers in the Earth-Moon System*. Ph.D. Dissertation, University of Colorado, Boulder, Colorado, 2015.

[7] N. L. Parrish, J. S. Parker, S. P. Hughes, and J. Heiligers, "Low-Thrust Transfers From Distant Retrograde Orbits To L2 Halo Orbits in the Earth-Moon System," *International Conference on Astrodynamics Tools and Techniques*, Darmstadt, Germany, 2016, pp. 1–9.

[8] D. Guzzetti, E. M. Zimovan, K. C. Howell, and D. C. Davis, "Stationkeeping Analysis for Spacecraft in Lunar Near Rectilinear Halo Orbits," *27th AAS/AIAA Space Flight Mechanics Meeting*, San Antonio, Texas, February 5 – 9, 2017.

[9] M. McGuire, L. Burke, S. McCarty, K. J. Hack, R. Whitley, D. C. Davis, and C. Ocampo, "Low Thrust Cis-Lunar Transfers Using a 40 kW-Class Solar Electric Propulsion Spacecraft," *AAS/AIAA Astrodynamics Specialist Conference 2017*, Stevenson, Washington, August 2017.

[10] S. L. McCarty and M. L. McGuire, "Parallel Monotonic Basin Hopping for Low Thrust Trajectory Optimization," *AIAA SciTech Forum*, Kissimmee, Florida, January 2018.

[11] G. Lantoine, "Efficient NRHO to DRO Transfers in Cislunar Space," *AAS/AIAA Astrodynamics Specialist Conference*, Stevenson, Washington, August 2017.

[12] E. M. Zimovan, K. C. Howell, and D. C. Davis, "Near Rectilinear Halo Orbits and Their Application in Cis-Lunar Space," *3rd International Academy of Astronautics Conference on Dynamics and Control of Space Systems*, Moscow, Russia, May 30 – June 1, 2017.

[13] E. M. Zimovan, "Characteristics and Design Strategies for Near Rectilinear Halo Orbits within the Earth-Moon System," M.S. Thesis, School of Aeronautics and Astronautics, Purdue University, West Lafayette, Indiana, August 2017.

[14] D. C. Davis, K. K. Boudad, R. J. Power, and K. C. Howell, "Heliocentric Escape and Lunar impact from Near Rectilinear Halo Orbits," *2019 AAS/AIAA Astrodynamics Specialist Conference*, Portland, Maine, August 11 – 15, 2019.

[15] N. Bosanac, *Leveraging Natural Dynamical Structures to Explore Multi-Body Systems*. Ph.D. Dissertation, Purdue University, West Lafayette, Indiana, 2016.

[16] E. Campbell, *Bifurcations from Families of Periodic Solutions in the Circular Restricted Problem with Application to Trajectory Design*. Ph.D. Dissertation, Purdue University, West Lafayette, Indiana, 1999.

[17] R. Broucke, "Stability of Periodic Orbits in the Elliptic, Restricted Three-Body Problem," *AIAA Journal*, Vol. 7, No. 6, 1969, pp. 1003–1009.

[18] D. Grebow, *Trajectory Design in the Earth-Moon System and Lunar South Pole Coverage*. Ph.D. Dissertation, Purdue University, West Lafayette, Indiana, 2010.

[19] J. Crusan, "Gateway Update: NASA Advisory Council, Human Exploration and Operations Committee," `https://www.nasa.gov/sites/default/files/atoms/files/20181206-crusan-gateway-reduced-v4.pdf`, 2018.

[20] D. C. Davis, K. K. Boudad, S. M. Phillips, and K. C. Howell, "Disposal, Deployment, and Debris in Near Rectilinear Halo Orbits," *29th AAS/AIAA Space Flight Mechanics Meeting*, Ka'anapali, Maui, Hawaii, January 13 – 17, 2019.

[21] A. D. Cox, N. Bosanac, D. Guzzetti, K. Howell, D. Folta, and C. Webster, "An Interactive Trajectory Design Enviornment Leveraging Dynamical Structures in Multi-body Regimes," *6th International Conference on Astrodynamics Tools and Techniques*, Darmstadt, Germany, March 14 – 17, 2016.

[22] D. Folta, N. Bosanac, D. Guzzetti, and K. Howell, "An Earth-Moon System Trajectory Design Reference Catalog," *2nd AIAA Conference on Dynamics and Control of Space Systems*, Roma, Italy, March 24 – 26, 2014.

[23] D. Folta, C. Webster, N. Bosanac, A. D. Cox, D. Guzzetti, and K. Howell, "Trajectory Design Tools for Libration and Cislunar Environments," *6th International Conference on Astrodynamics Tools and Techniques*, Darmstadt, Germany, March 14 – 17, 2016.

[24] D. Guzzetti, N. Bosanac, A. Haapala, K. Howell, and D. Folta, "Rapid Trajectory Design in the Earth-Moon Ephemeris System via an Interactive Catalog of Periodic and Quasi-Periodic Orbits," *Acta Astronautica*, Vol. 126, September-October 2016, pp. 439–455.

[25] R. Pritchett, E. Zimovan, and K. C. Howell, "Impulsive and Low-Thrust Transfer Design between Stable and Nearly Stable Periodic Orbits in the Restricted Problem," *18th AIAA SciTech Forum*, Kissimmee, Florida, January 8 – 12, 2018.